

SIGN UP FOR ALERTS **Physics of Fluids** 

AIP Physics of Fluids



SUBMIT YOUR ARTICLE

HOME BROWSE INFO FOR AUTHORS

 SIGN UP FOR ALERTS

COLLECTIONS

Home > Physics of Fluids > Volume 30, Issue 5 > 10.1063/1.5026404



< PREV NEXT >

Full . Published Online: 02 May 2018 Accepted: April 2018

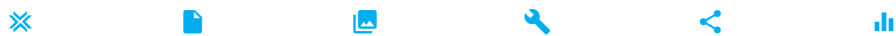
Magnetohydrodynamic pressure drop and flow balancing of liquid metal flow in a prototypic fusion blanket manifold

Physics of Fluids **30**, 057101 (2018); <https://doi.org/10.1063/1.5026404>

Tyler J. Rhodes, Sergey Smolentsev, *and* Mohamed Abdou

Hide Affiliations

Mechanical and Aerospace Engineering Department, University of California Los Angeles, 44-114 Engineering IV, 420 Westwood Plaza, Los Angeles, California 90095-1597, USA



- Topics ▾
 - Topics ▲
 - Fluid flows
 - Fusion reactors
 - Liquid metals
 - Electric currents
 - Vector fields
 - Electromagnetism
 - Hydrodynamical interactions
 - Magnetohydrodynamics

ABSTRACT

Understanding magnetohydrodynamic (MHD) phenomena associated with the flow of electrically conducting fluids in complex geometry ducts subject to a strong magnetic field is required to effectively design liquid metal (LM) blankets for fusion reactors. Particularly, accurately predicting the 3D MHD pressure drop and flow distribution is important. To investigate these topics, we simulate a LM MHD flow through an electrically non-conducting prototypic manifold for a wide range of flow and geometry parameters using a 3D MHD solver, HyPerComp incompressible MHD solver for arbitrary geometry. The reference manifold geometry consists of a rectangular feeding duct which suddenly expands such that the duct thickness in the magnetic field direction abruptly increases by a factor r_{exp} . Downstream of the sudden expansion, the LM is distributed into several parallel channels. As a first step in qualifying the flow, a magnitude of the curl of the induced Lorentz force was used to distinguish between inviscid, irrotational core flows and boundary and internal shear layers where inertia and/or viscous forces are important. Scaling laws have been obtained which characterize the 3D MHD pressure drop and flow balancing as a function of the flow parameters and the manifold geometry. Associated Hartmann and Reynolds numbers in the computations were $\sim 10^3$ and $\sim 10^1$ - 10^3 , respectively, while r_{exp} was varied from 4 to 12. An accurate model for the pressure drop was developed for the first time for inertial-electromagnetic and viscous-electromagnetic regimes based on 96 computed cases. Analysis shows that flow balance can be improved by lengthening the distance between the manifold inlet and the entrances of the parallel channels by utilizing the effect of flow transitioning to a quasi-



Scilight

Brief summaries of the best new articles in the **physical sciences**

Sign up for free!

AIP Publishing

The banner features a dark gold background with abstract, glowing light patterns. The text is white and centered, with 'Scilight' at the top, followed by a descriptive sentence, a call to action, and the AIP Publishing logo at the bottom.

two-dimensional state in the expansion region of the manifold.

I. INTRODUCTION

Any liquid metal (LM) blanket of a power fusion reactor, for instance a US Dual Coolant Lead Lithium (DCLL) blanket,¹ exhibits a variety of complex geometry flows, including flows in bends, contractions, expansions, elbows, etc., where a liquid metal breeder circulates in the presence of a strong plasma-confining magnetic field for cooling, power conversion, and tritium breeding. Among them, manifolds are the key 3D elements as they are responsible for distributing the liquid inside the blanket. Such manifolds distribute the LM flow from a radial feeding pipe at the blanket inlet to several poloidal channels and, vice versa, collect the liquid from the poloidal flows to an exit pipe at the blanket outlet. Though these manifolds are small compared to the full length of the liquid metal circuit, they are known to be the main contributors to the pressure drop in the blanket due to 3D magnetohydrodynamic (MHD) effects that occur near sudden changes in the blanket geometry.² Reducing the pressure drop of the circulating breeder is one of the most fundamental practical goals of the blanket design and analysis. Additionally, it is important that the LM is distributed evenly throughout the blanket. Therefore, it is important to understand and quantify the 3D effects in the manifold flows relating to MHD pressure drop and flow distribution. These 3D MHD effects are associated with 3D induced electric currents that close their circuit mostly in the axial direction. The electromagnetic Lorentz forces associated with the 3D currents are responsible for complex 3D flow

patterns, formation of boundary and internal MHD layers, 3D pressure gradients, and ultimately, high extra pressure losses.

3D MHD effects are known to be caused by non-uniform applied magnetic fields and, as in the present work, by axial variations of the flow geometry.² By comparison, 2D MHD effects are associated with 2D electric currents that circulate in the cross-sectional plane perpendicular to the main flow direction. The 2D effects are typical of fully developed MHD flows, in which the velocity field does not change with the axial coordinate while the pressure varies linearly in the axial direction without variation within the cross-sectional plane. A number of analytic solutions (e.g., Refs. 3 and 4) are available for predicting 2D MHD flows, whereas 3D MHD flows are much more complicated such that the 3D MHD pressure drops must be determined experimentally or via numerical modeling.

In the present work, we perform 3D numerical analysis of MHD flows in a simplified model of the inlet manifold subject to a transverse magnetic field (Fig. 1).

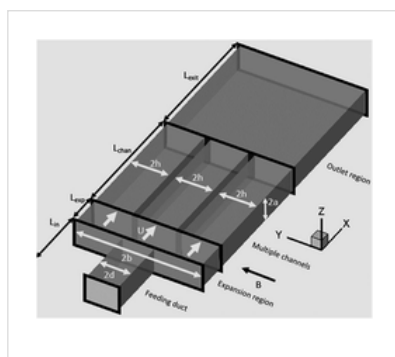


FIG. 1. A prototypic manifold geometry for numerical simulation. Fully developed flow

enters the feeding duct, spreads out into the expansion region, is sorted into multiple parallel channels, and collects in the common outlet where it becomes fully developed before exiting the duct.

In this prototypic model, the flow enters the manifold of height $2a$ through the feeding duct of width $2d$ and length L_{in} before entering the expansion region, which has length L_{exp} , width $2b$, and average velocity U . From the expansion region, the flow proceeds into three or more identical parallel channels of the width $2h$ and length L_{chan} and exits through a common outlet of width $2b$ and length L_{exit} . These dimensions have a strong effect on the flow distribution and the pressure drop and are subject to optimization. In the present study, some of the dimensions were used as computational parameters to address the effect of the manifold design on the flow. The flow in the manifold occurs in a uniform transverse magnetic field B , which was also used as a parameter in the computational study. In this study, we limit our consideration to a non-conducting manifold such that all induced electric currents are closed inside the flow domain.

The obtained numerical data were then used to qualify the manifold flow physics in a wide range of flow parameters relevant to a LM blanket and to eventually approximate the computed pressure drops in the form of simple correlations. These correlations for the 3D MHD pressure drop in the manifold flow were constructed for the first time using linear regression analysis to express the pressure drop as a function of the manifold expansion ratio, r_{exp} , Hartmann number, Ha (Ha^2 is the ratio of electromagnetic to viscous force), and interaction parameter, N (ratio of electromagnetic to inertia force) which is equal to Ha^2/Re , where Re is the Reynolds number (ratio of inertia to viscous force). The proposed pressure drop model can be

recommended to evaluate the pressure drop in the manifold of a DCLL blanket or other LM blankets at fusion relevant parameters.

Previous 3D MHD pressure drop estimations for blanket manifolds relied on empirical correlations in the form $\Delta P_{3D} = \zeta(0.5)\rho U^2$, where ζ , the local pressure drop coefficient, is proportional to N .^{5,6} The semi-empirical model proposed in this study is a significant step forward as it relates the pressure loss to the theory for the internal MHD shear layers parallel to the magnetic field that can be formed near abrupt changes in the flow. Hunt and Leibovich first coined the term “Ludford layer” to describe such internal layers that span the flow at locations where the walls not parallel to the magnetic field have sufficiently high curvature.⁷ Their 2D asymptotic analysis of Ludford layers suggested the existence of essentially three possible flow regimes which are characterized by the forces that balance the pressure gradient inside the Ludford layer: (i) the viscous-electromagnetic (VE) regime which holds for $N \gg Ha^{3/2}$, (ii) the inertial-electromagnetic (IE) regime for $N \ll Ha^{3/2}$, and a third regime (iii) where all three forces, inertial-viscous-electromagnetic (IVE), are balanced for $N \sim Ha^{3/2}$. The pressure drop across the Ludford layer (in the MHD scale [$p^* = p/\sigma UB^2 b$]) scales with $Ha^{-1/2}$, or $N^{-1/3}$, or either (since $Ha^{-1/2} = N^{-1/3}$ when $N = Ha^{3/2}$) for the VE, IV, and IVE regimes, respectively.⁸ Although the problem formulation in Ref. 7 is not fully consistent with real 3D duct flows, the conclusions listed above have been applied successfully to 3D flows. Several authors⁹⁻¹² have pointed to Ludford layer theory to explain the scaling behavior of 3D MHD pressure drops and internal shear layer thickness in 3D complex geometries, including sudden expansions and 90° bends. In this paper, numerically determined

correlations for 3D MHD pressure drops are shown to agree with the same scaling arguments which are validated by these previous studies. The correlations provided in the present work are unique in that they are valid for non-conducting ducts with variable expansion ratio to be useful for designing LM manifolds.

An important function of the inlet manifold is to distribute the liquid uniformly among the parallel channels because the flow imbalance can cause unacceptable overheating in underfed channels. As shown in this study, the flow in the expansion region tends to become quasi-two dimensional (Q2D) under the effect of a strong transverse magnetic field and therefore tends to be spread uniformly among the parallel channels. However, the flow in the expansion region contains 3D flow such that manifold designs featuring short expansion regions may result in uneven flow distributions. On the other hand, the flow distribution is also affected by the length of the parallel channels.¹³ The practical question is how to design a manifold to minimize the flow imbalance. An answer to this important question and practical recommendations were also given in this study based on the 47 computed cases and their analysis.

The paper is organized as follows: Sec. II contains a description of the problem formulation and numerical methods used; Sec. III contains a brief comparison to experimental results, a mesh refinement study, a discussion of the physics and phenomena of MHD manifold flows, a discussion of the developed 3D MHD pressure drop model, a discussion of the flow distribution in manifolds, and an example application of the developed pressure model to a DCLL blanket; Sec. IV contains a summary of conclusions.

II. PROBLEM FORMULATION, NUMERICAL CODE, AND COMPUTATIONAL MESH

To study 3D MHD manifold flow behavior sketched in Fig. 1, a well-verified MHD solver developed by HyPerComp/UCLA, (HyPerComp Incompressible MHD solver for Arbitrary Geometry) HIMAG,¹⁴ was used to simulate the laminar flow of liquid metal of kinematic viscosity ν , electrical conductivity σ , and density ρ through an electrically insulated manifold in a strong transverse magnetic field B . Such a flow is characterized by the following key dimensionless parameters: the Hartmann number, $Ha = bB\sqrt{\sigma\nu\rho}$; the Reynolds number, $Re = \frac{bU}{\nu}$; the expansion ratio, $r_{\text{exp}} = b/d$; the dimensionless length of the expansion region, L_{exp}/b ; the dimensionless length of the parallel channels, L_{chan}/b ; and the channel size parameter, $s_c = h/b$. In addition to Re and Ha , the interaction parameter, $N = \frac{Ha^2}{Re}$, which characterizes the ratio of electromagnetic to inertia forces, is another important parameter. The half width b of the expansion region was chosen as a length scale in the definition of Ha , Re , and N to best characterize the 3D MHD effects which exist primarily in the expansion region. Furthermore, the expansion region is also where the flow is redistributed and where stationary vortex tubes may exist. For the same reasons, the average velocity in the expansion region U was chosen as the velocity scale. However, because the flow in the expansion region is electrically coupled with the flow in the inlet via 3D currents, the expansion ratio r_{exp} is required in order to fully characterize the flow. Physical properties were chosen to equal those of eutectic lead-lithium alloy (PbLi) at 500 °C. The applied magnetic field B was varied to control Ha . U was chosen such that the inlet velocity $U^*r_{\text{exp}} = 0.01$ m/s is the same for all the simulations and $\frac{a}{d} = 0.8$ for every simulation.

The HIMAG code solves the full incompressible MHD equations, shown below [(1)–(4)], using an electric potential formulation with the assumption that the induced magnetic field is small enough to be neglected compared to the applied one.

Equations (1)–(4) are the modified form of the Navier-Stokes-Maxwell equations written in the inductionless approximation, which include the continuity equation, momentum equation with the Lorenz force term on the right-hand side, Ohm’s law to compute the induced electric current, and the electric potential equation, respectively,

$$\nabla \cdot \mathbf{u} = 0, \quad (1)$$

$$\frac{\partial \mathbf{u}}{\partial t} + \mathbf{u} \cdot \nabla \mathbf{u} = -\frac{1}{\rho} \nabla p + \nu \nabla^2 \mathbf{u} + \frac{1}{\rho} \mathbf{J} \times \mathbf{B}, \quad (2)$$

$$\mathbf{J} = \sigma (-\nabla \phi + \mathbf{u} \times \mathbf{B}), \quad (3)$$

$$\nabla \cdot (\sigma \nabla \phi) = \nabla \cdot (\sigma \mathbf{u} \times \mathbf{B}). \quad (4)$$

Here, \mathbf{u} , \mathbf{J} , and \mathbf{B} are the velocity, electric current density, and magnetic field vectors, respectively, and p and ϕ are the pressure and electric potential. Equation (4) is obtained by taking the divergence of Eq. (3) while stipulating that electric current is continuous ($\nabla \cdot \mathbf{J} = 0$). To consider both the liquid and the surrounding solid wall, which may have different electrical conductivity, the electrical conductivity σ is put inside the derivatives in Eq. (4).

HIMAG (HyPerComp Incompressible MHD solver for Arbitrary Geometry) is a three-dimensional, unstructured grid-based MHD flow solver developed over the last decade by a US software company named HyPerComp, with support from UCLA. The numerical approach is based on finite-volume discretization using a collocated

arrangement (all unknowns are located at the cell centers) with second-order accuracy in space and time. The mass conservation is satisfied, and the pressure field is evaluated using a four-step projection method with the semi-implicit Crank–Nicolson formulation for the convective and diffusion terms. A charge conserving consistent scheme developed in Refs. 15 and 16 is applied to accurately compute the electric potential and the electric current density at high Hartmann numbers. Given the unstructured nature of the solver, multiple strategies are employed to account for mesh skewness and non-orthogonality. Finally, the solver algorithms are parallelized using the Message Passing Interface (MPI) architecture, thereby making the solver capable of being run on large computational clusters. Additional details regarding the formulation and validation of the HIMAG code can be found elsewhere (e.g., Ref. 17).

Equations (1)–(4) were solved numerically on non-uniform rectangular meshes (Fig. 2). In making each mesh, we ensured that there are at least 5 nodes inside all Hartmann layers on the walls perpendicular to the magnetic field and 12 nodes inside each side layer on the wall parallel to the magnetic field. Also, higher mesh resolution was used in the liquid next to the back wall of the expansion region, which is perpendicular to the axial direction, and at the beginning and end of the multiple channels.

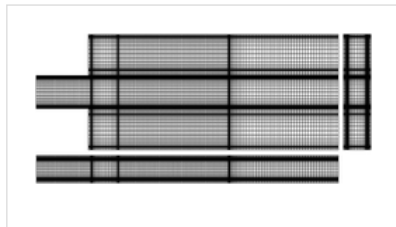


FIG. 2.
An example
computational
mesh with 2.05×10^6 cells for a

manifold geometry with 3 channels, $L_{\text{exp}}/b = 0.5$, $L_{\text{chan}}/b = 2$, $r_{\text{exp}} = 4$, and $s_c = 0.3$.

Shercliff flow³ is used at the inlet boundary condition for both the pressure gradient and the velocity profile in the feeding duct and a fully developed flow outlet boundary condition in the form $\frac{\partial}{\partial x} = 0$ is used at the exit. The pressure is set to zero at the outlet and the fluid-wall boundaries have Neumann pressure conditions $\left(\frac{dp}{dn} = 0\right)$. The no slip and no flow-through conditions are enforced at fluid-wall interfaces ($\mathbf{u}_{\text{wall}} = \mathbf{0}$). Normal components of electric current density are set to zero at the outer domain boundary $\left(\frac{d\phi}{dn} = (\mathbf{u} \times \mathbf{B}) \cdot \hat{\mathbf{n}}\right)$. Since this study deals with a non-conducting manifold, the wall electrical conductivity is set to zero. Simulations were started with initially uniform flow conditions with a time step size of $\Delta t = 10^{-4}$ s. Using the Hoffman2 computer cluster at UCLA, each simulation was run in parallel on 64 or 128 nodes until steady state solutions were reached as determined by the L2 norm of the residuals reaching the order of 10^{-10} . The L2 norms of residuals were calculated according to the following equations:

$$|\mathbf{r}| = \sqrt{\sum_i^2 r_i^2}, \quad (5)$$

$$r_i = F_i^{m+1} - F_i^m. \quad (6)$$

Here the L2 norm $|\mathbf{r}|$ of residuals r_i is calculated for each of the flow variables F for time step m . The subscript i is the cell index. Many simulations varying by geometry and Ha were started simultaneously. Once each simulation converged, the converged solutions were used as initial conditions for subsequent simulations at higher values of the flow parameters to reduce the

computational time. Totally, 130 cases have been computed. The minimal computational time was half a day and the longest simulations ran for a month, depending on the flow parameters and manifold geometry. Generally, computational time increased as Re was increased.

III. RESULTS AND DISCUSSION

A. Comparison to previous results and mesh refinement study

Present simulation results show superior agreement with the experimental measurements and demonstrate significant improvement compared to the previous computations of flow distribution in an MHD manifold. Figure 3 shows the flow distribution for a manifold that feeds three channels as determined by experimental work by Messadek and Abdou at UCLA,¹⁸ numerical work by Morley *et al.*,¹⁹ and the present numerical work.

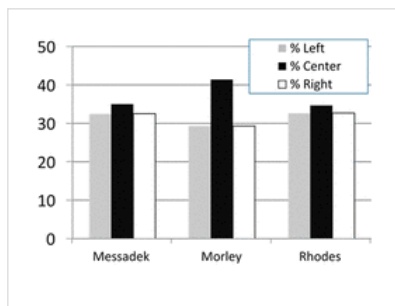


FIG. 3. A comparison of present simulation results with previous numerical and experimental work.¹⁷ Here flow distribution is reported as the percentage of flow through each of three channels. $Ha = 2190$, $Re = 250$, $r_{exp} = 4$, $L_{chan}/b = 2$, $L_{exp}/b = 1$, and $s_c = 0.3$.

[↓ PPT](#) | [High-resolution](#)

The computations done in the present study show just a small imbalance among three parallel

channels (for the given set of the parameters). This is very similar to the earlier experiments but different from the computational predictions in Ref. 19. The recent improvement in the computations of the manifold flows is attributed solely to the addition of a common outlet region with length L_{exit} so that the use of the uniform pressure boundary condition ($p = 0$) is more appropriate. In the previous computations in Ref. 19, the outlet section was not included such that the flow at the manifold exit was artificially forced to agree with the uniform pressure boundary condition.

Prior to the main computations, a mesh sensitivity study was performed using an electrically non-conducting manifold without multiple channels at $Ha = 4380$, $Re = 100$, and $r_{exp} = 8$ on three computational meshes of $\sim 10^6$ cells each in order to quantify the discretization error, including “coarse,” “medium,” and “fine” meshes. Each consecutive mesh featured approximately twice as many cells as the previous mesh. The number of cells in each mesh is shown in Table I.

TABLE I. Mesh refinement details.

The manifold’s centerline axial pressure gradient obtained in the mesh sensitivity study for the three meshes is plotted in Fig. 4 along with the fully developed flow Shercliff solution.

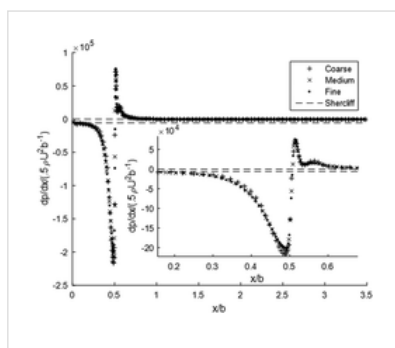


FIG. 4. Results of a mesh refinement study. Axial pressure gradient is plotted along the $y = z = 0$

centerline of a manifold without multiple channels for three meshes: coarse, medium, and fine. Fully developed flow Shercliff solution is also shown. Zooming in on the sudden expansion at $x/b = 0.5$ reveals differences between the meshes. Here, $Ha = 4380$, $Re = 100$, and $r_{exp} = 8$.

[↓ PPT | High-resolution](#)

The difference in the pressure drop between the medium mesh and the coarse mesh is 2.55%. The difference in the pressure drop between the fine mesh and the medium mesh is 0.027%. For all other computations in the present work, meshes similar to the fine mesh are used.

B. Characterization of the flow

Before going into details of the proposed pressure model and flow distribution analysis, we first summarize here the most important flow features to better understand the fundamental manifold flow physics. The discussion is based on the present computations for electrically non-conducting manifold as shown in Fig. 1 in a range of flow parameters relevant to a fusion blanket at $Ha \sim 10^3$, $r_{exp} \geq 4$, and $Re \sim 10^1-10^3$. In this parameter space, the computed flows are laminar, symmetrical with respect to the symmetry planes $y = 0$ and $z = 0$, and steady. The most characteristic flow feature, as we can observe in all our computations, is the appearance of induced 3D (axial) currents as shown in Fig. 5 and related 3D MHD effects that manifest themselves through abrupt variations in the velocity and pressure field where the flow geometry changes.

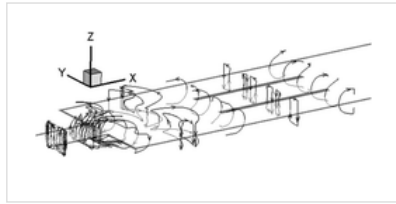


FIG. 5.
Electric currents circulate in an MHD manifold

flow. The currents become 3D near changes in the flow geometry. $r_{\text{exp}} = 4$, $L_{\text{exp}}/b = 2$, $L_{\text{chan}}/b = 2$, $s_c = 0.3$, and $n = 3$ channels for $Ha = 1465$ and $Re = 50$.

[↓ PPT](#) | [High-resolution](#)

Sources for the 3D MHD effects exist at three locations along the flow path (see the sketch in Fig. 1): first when the liquid enters the expansion region, when it is distributed into parallel channels, and then near the exit of the channels when the liquid is collected before exiting the manifold. The generation of such 3D currents at these three locations can be explained through Ohm's law. Namely, the average velocity changes due to continuity as the flow geometry changes. These changes in the mean velocity (while the applied magnetic field does not change) cause axial variations in the electric potential distribution which in turn drive an axial electric current whose circuit is closed upstream and downstream of each cross-sectional variation. This phenomenon is illustrated in detail for the sudden expansion in Fig. 6.

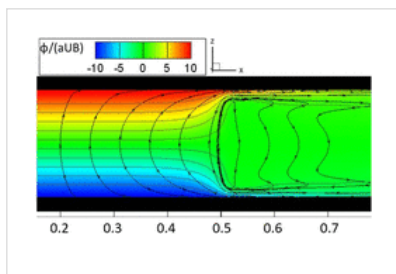


FIG. 6.
Electric potential and currents on the $y = 0$ center plane. Axial currents are

generated near the sudden expansion at $x/b = 0.5$ and then close upstream and downstream

of the expansion. $Ha = 5475$, $Re = 50$, and $r_{exp} = 10$.

[↓ PPT | High-resolution](#)

Such 3D circulations are shown to occur where the mean velocity decreases across the sudden expansion, increases into each individual parallel channel, and then decreases again into the outlet region. Compared to 2D currents which are limited by the resistance of the Hartmann layers where they close, 3D currents mostly close inside the bulk of the fluid. As a result, even small changes in the cross section cause bulk current densities that are much greater than the 2D circulations which occur in the feeding duct near the inlet, in the middle of the parallel channels, and near the end of the outlet region as shown in Fig. 5.

The observed 3D and 2D current circuits and associated Lorentz forces have a strong impact on the flow and the pressure field as illustrated in Fig. 7, which shows velocity profiles at nine selected locations along the flow path as well as the axial pressure distribution.

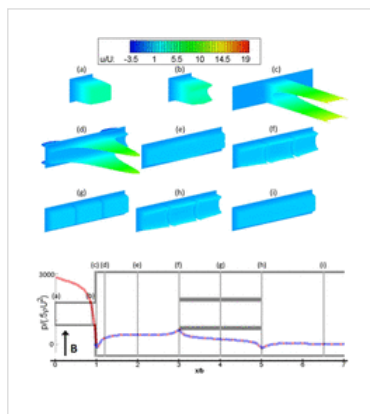


FIG. 7.

(Bottom) Non-dimensional pressure is plotted for the centerlines of the center (solid red) and side (dashed blue)

channels over a top-down view (xy) of a manifold with $r_{exp} = 4$, $L_{exp}/b = 2$, $L_{chan}/b = 2$, $s_c = 0.3$, and $n = 3$ channels for $Ha = 1465$ and $Re = 50$. The vertical gray lines labeled (a) through (i) correspond to the 9 axial velocity profiles

shown above. (Top) Non-dimensional axial component of velocity, u/U , is plotted for yz cross sections at 9 locations along the manifold.

[↓ PPT](#) | [High-resolution](#)

Inside the feeding duct, the 3D MHD effects are responsible for smoothly transitioning the flow from a fully developed Shercliff velocity profile at the inlet [location (a) in Fig. 7] to an M-shaped profile [location (b)]. The trend of forming the M-shaped velocity profile accelerates rapidly between locations (b) and (c) and falls off just as quickly downstream of the expansion. Inside the expansion region, a complex M-shaped flow structure [location (d)] quickly changes to a nearly uniform flow, evenly distributed in the transverse direction [location (e)], owing to the tendency of MHD duct flows in a strong transverse magnetic field to become quasi-2D. The 3D effects reappear at locations (f) and (h) at the entry to and at the exit from the parallel channels. Inside the parallel channels, between locations (f) and (h), the flow is almost fully developed as seen from the linear pressure distribution and Shercliff-type velocity profiles at location (g). Once exiting the parallel channels, the flow in the outlet region quickly becomes fully developed [location (i)].

The flow downstream of the sudden expansion [between locations (c) and (e)] is particularly complex and warrants further discussion. The flow enters the expansion region with the majority of the flow localized near the side walls parallel to the magnetic field [Fig. 7(c)]. In the side layers, y -direction pressure gradients force flow outwards toward the periphery of the channel. The y -direction pressure gradients are induced by axial electric currents as follows: axial currents exist near

the side walls as seen in Fig. 8(a) which cause the z -direction Lorentz force in the expansion region; according to the direction of the axial currents here, these forces are positive near the center and negative near sides (at $|y| > 0$); as the core pressure is uniform along the y -direction, the side wall pressure will be greater near the center and lesser near the sides compared to the core pressure due to the z -direction Lorentz forces. The pressure on the side wall gradually becomes uniform as the axial current density approaches zero away from the expansion. The resulting pressure distribution near the side walls causes the liquid to return to the back wall of the expansion region in a manner that also distributes it along the y -direction as illustrated in Fig. 8(b). Once the fluid reaches the internal layer along the back wall, it drops out of the side layers to enter the Q2D core.

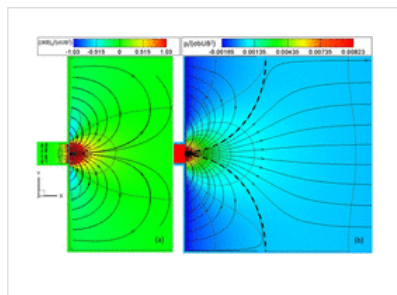


FIG. 8.
 (a) Electric currents and contours of z -direction Lorentz force at the $z/a =$

0.94 plane in the side layer. (b) Velocity streamlines and pressure contours at the $z/a = 0.94$ plane in the side layer. The dashed lines are streamlines which intersect the Hartmann walls at reattachment points and define a reattachment length. $r_{\text{exp}} = 10$, $Ha = 5475$, and $Re = 50$.

↓ PPT | [High-resolution](#)

The present observations of the reverse flow in the side layers are consistent with those of Bühler,²⁰ who first observed the reverse flow in MHD sudden

expansions, and of Mistrangelo,¹² who studied the reverse flow in more detail. Mistrangelo also defined the attachment length as the distance between a sudden expansion and a limiting streamline which bounds the reverse flow. She noted that the attachment length shrinks with a stronger applied magnetic field, scaling with $N^{-1/3}$. The electromagnetically driven 3D flow structure in the expansion region allows the core to become Q2D after a very short distance into the expansion region [note the evenly distributed core flow in Fig. 7(d)]. Past the attachment length, the entire flow in the expansion region becomes Q2D. The above description of the flow structure in the expansion region is typical for the entire parameter space of our simulations; however, at large enough Re , additional complexity enters the flow in the expansion region as stationary vortex tubes are observed to form (see Fig. 9).

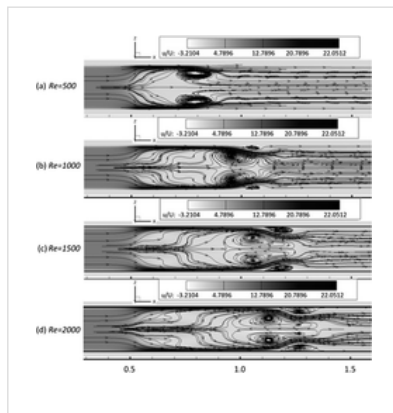


FIG. 9.
Velocity streamlines in the $y = 0$ center xz -plane of an insulating duct with a sudden expansion at x/b

$= 0.5$. $r_{\text{exp}} = 8$, $Ha = 3400$, and $Re = [500, 1000, 1500, 2000]$ for (a)-(d), respectively. The contours are of x -direction velocity.

[↓ PPT](#) | [High-resolution](#)

In the course of computations, the vortices were observed to travel downstream until steady state was achieved. The equilibrium axial position of the vortices is observed to increase with Re . The

number of vortices also increases as Re increases. The vortex tubes span the duct along magnetic field lines, confirming that the Q2D flow regime is dominant in the bulk of the flow despite the complexity.

Apart from the above considerations that refer to 2D versus 3D flow features, it is useful to look at the structure of MHD flows in the manifold from the point of view of the magnitude of curl of the Lorentz force. As shown below, a high magnitude of $\nabla \times \mathbf{J} \times \mathbf{B}$ indicates special flow subdomains, where inertial and/or viscous forces are important.²¹ To begin, we note that in the fusion relevant parameter space, $N \gg 1$ and $Ha \gg 1$ so that the flow is essentially inertialess and inviscid and pressure gradients tend to balance electromagnetic forces wherever possible. Such flow subdomains where viscous and inertia forces can be neglected are usually referred to as “core flows.”²² However, there can be subdomains where the Lorentz force cannot be fully balanced by the pressure gradients because pressure gradients are always curl free while the Lorentz force can include a rotational component. Thus, in such subdomains where its curl is non-zero, rotational hydrodynamic forces must exist to balance the Lorentz force. For instance, in fully developed MHD flows, the Lorentz force is curl free everywhere except for inside the Hartmann boundary layers at the walls perpendicular to the magnetic field and Shercliff layers at the duct walls parallel to the magnetic field, where viscous forces are very important. In uniform magnetic fields, $\nabla \times \mathbf{J} \times \mathbf{B}$ reduces to $(\mathbf{B} \cdot \nabla)\mathbf{J}$ so the curl of the Lorentz force can be interpreted as a measure of nonuniformity of current density along the B-field direction. Thus we can predict that the Lorentz force will be strongly rotational at expansions and contractions that

occur in the plane parallel to \mathbf{B} (as in the present case) because variation in current density is expected to occur along the B-field. The same cannot be said for expansions and contractions that are perpendicular to \mathbf{B} .

Plots of the magnitude of $\nabla \times \mathbf{J} \times \mathbf{B}$ in Fig. 10 confirm this prediction and reveal thin internal layers at the sudden expansion and contractions where viscous and inertial forces must be significant to balance electromagnetic forces. According to the 2D Ludford layer theory,⁷ and also as confirmed for 3D flows by Bühler²⁰ and Mistrangelo,¹² the thickness δ of the internal layer scales with $Ha^{-1/2}$ if the flow regime is viscous-electromagnetic for $N \gg Ha^{3/2}$ and with $N^{-1/3}$ in the inertial-electromagnetic regime for $N \ll Ha^{3/2}$. In the literature, the internal layer is also sometimes referred to as the expansion layer, a term coined by Bühler to differentiate the 3D phenomenon from the 2D Ludford layer. Here, we refer to these layers as internal layers. Figure 10 clearly demonstrates the formation of thin internal layers at the sudden expansion and at the entrance to and exit from the parallel channels. Hartmann and Shercliff boundary layers, where viscous forces are dominant, are also visible.

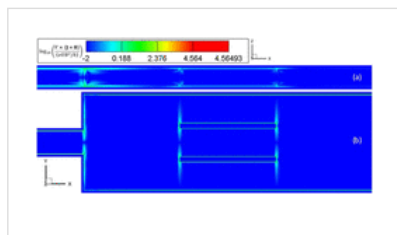


FIG. 10. Contours of the log of the magnitude of $\nabla \times \mathbf{J} \times \mathbf{B}$ are

shown on the $y = 0$ xz -plane (a) and on the $z = 0$ xy -plane (b) indicating that most of the manifold flow can be classified as a core flow except for special subdomains at the sudden expansion, entry to and exit from the parallel channels, as well as boundary layers where

rotational hydrodynamic forces are important. Here, $r_{\text{exp}} = 4$, $L_{\text{exp}}/b = 2$, $L_{\text{chan}}/b = 2$, $s_c = 0.3$, and $n = 3$ channels for $Ha = 1465$ and $Re = 50$.

[↓ PPT | High-resolution](#)

Unlike the thin internal and boundary layers highlighted by high magnitudes of $\nabla \times \mathbf{J} \times \mathbf{B}$, the magnitude of $\nabla \times \mathbf{J} \times \mathbf{B}$ is negligibly small in the core flows. When the liquid flows through the manifold, relatively large core flow subdomains are separated by thin internal layers. At such locations where $\nabla \times \mathbf{J} \times \mathbf{B}$ changes along the flow direction, large changes to the velocity field must also occur to generate sufficient hydrodynamic forces.²³ In support of this claim, we observe the formation of M-shaped velocity profiles [Figs. 7(c), 7(f), and 7(h)] near each change in the duct cross section. For example, in the feeding pipe, the flow slowly transitions from a fully developed Shercliff velocity profile at the inlet [Fig. 7(a)] to an M-shaped profile [Fig. 7(b)] as the velocity in the core decreases and the velocity near the side walls increases. Then, over a short distance where strong $\nabla \times \mathbf{J} \times \mathbf{B}$ appears in the flow, the velocity profile quickly becomes severely M-shaped and 3D [Fig. 7(c)]. Away from each change in cross section, the flow transitions toward a fully developed Shercliff velocity profile [Figs. 7(a), 7(e), 7(g), and 7(i)]. The formation of M-shaped velocity profiles at expansions was first observed in experiments performed at Riga by Branover and Shcherbinin²⁴ and was later studied analytically by Walker, Ludford, and Hunt²⁵ and observed numerically by many authors.^{26-30,20,12,19}

The pressure distribution in the manifold flow is of special interest as typically high MHD pressure drops in fusion blankets exert critical limitations on

any liquid metal blanket design. As shown in Fig. 7 at the bottom, the pressure is distributed non-uniformly along the flow path: local minimums in axial pressure are observed at expansions while contractions experience local maximums. These pressure features arise due to the 3D currents which rotate in opposite directions at expansions compared to contractions. At expansions, Lorentz forces push outwards away from the center of the 3D circulations and so the balancing pressure gradients pinch inwards, creating a local pressure minimum. The reverse situation occurs at contractions. The same explanation accounts for high side wall pressure (relative to the bulk) at expansions and low side wall pressure at contractions.

As seen in the axial pressure distribution shown in Fig. 7, the most significant changes in the pressure occur at the sudden expansion at $x/b = 1$ because of strong 3D MHD effects associated with the expansion of the flow along the y -direction. The pressure drop which occurs at the sudden expansion is considerably larger than the pressure recovery which follows just downstream. The net effect is referred to as the 3D MHD pressure drop. A sketch explaining the definition of the 3D MHD pressure drop in the flow with a sudden expansion is shown in Fig. 11 as originally proposed by Bühler.²⁰

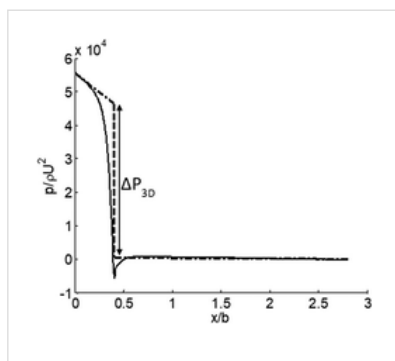


FIG. 11.

The length of the vertical dashed line at the sudden expansion is defined as the 3D MHD pressure

drop in the hydraulic scale. The two dashed-dotted black lines have slopes equal to the local

fully developed Shercliff pressure gradient.

Here, $r_{\text{exp}} = 10$, $Ha = 5475$, and $Re = 50$.

[↓ PPT](#) | [High-resolution](#)

This large axial pressure drop across the sudden expansion has two explanations. First, the current density of 3D circulations (and thus axial Lorentz force) is greater upstream of the expansion because the currents spread out into the expansion region as they close downstream. This is sufficient for explaining the centerline pressure distribution since $\nabla \times \mathbf{J} \times \mathbf{B}$ is zero on the centerline (by symmetry) and so the pressure gradient is nearly entirely balanced by the Lorentz force. A more general explanation for the 3D MHD pressure drop is that extra momentum is lost to the walls near the expansion due to 3D flow structures and the formation of near wall jets [e.g., Fig. 7(c)]. The scaling of the 3D MHD pressure drop across sudden expansions was first proposed by Molokov⁹ and was later confirmed numerically by Mistrangelo¹² for the IE regime and again numerically in the present work (Sec. III C) for both the VE and IE regimes.

C. Pressure analysis

We now go on to discuss our numerical investigation of the 3D MHD pressure drop which is inserted into the flow near the sudden expansion. We numerically determine the 3D MHD pressure drop to scale linearly with $\rho U^2 N^{2/3}$ and $\rho U^2 N H a^{-1/2}$ for the IE and VE regimes, respectively, indicating agreement with the predictions of Molokov⁹ who based his conclusions on the scaling arguments made by Hunt and Leibovich⁷ in their analysis of the Ludford layer in

2D. We also conclude that the 3D MHD pressure drop has a strong dependence on r_{exp} .

Electrically non-conducting manifolds featuring a sudden expansion were simulated to study how the pressure drop changes with flow parameters and geometry. One of our hypotheses is that the influence of the multiple channels can be separated out of the pressure drop provided that the channel walls are not so thick that average velocity inside the channels is much higher than in the expansion region. More succinctly, disturbances caused by the entrances and exits of the multiple channels are expected to be small provided that the product $n \times s_c$ is close to unity, where n is the number of channels. Furthermore, the 2D MHD pressure drops across the channels are also relatively small while L_{chan} is small and $n \times s_c$ is close to unity. To test this hypothesis, we simulated two sets of manifolds with $Ha = 1000$, $r_{exp} = 4$, and $Re = [50, 500]$. One set of manifolds had $n = 3$ channels beginning at $L_{exp}/b = 1$, with $s_c = 0.3$ and $L_{chan}/b = 2$ while the other set of manifolds were simulated without multiple channels ($n = 1$, $s_c = 1$). The resulting pressure distributions are plotted along the centerlines in Fig. 12.

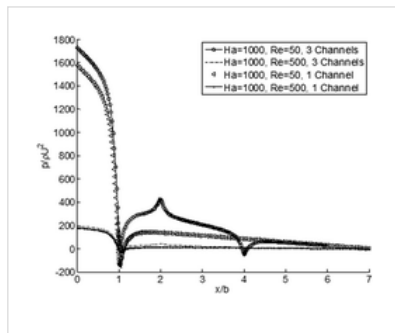


FIG. 12.
Centerline pressure of manifold simulations with either 1 or 3 channels, $r_{exp} = 4$.

For the cases with 3 channels, $L_{exp}/b = 1$, $L_{chan}/b = 2$, and $s_c = 0.3$. The flow with $Re = 50$ is in the VE regime and the $Re = 500$ flow is in the IE regime. Sudden expansion is at $x/b = 1$.

The local minima and maxima seen in Fig. 12 indicate locations where 3D MHD effects are generated. The local minima occur when the pressure gradient steepens and then abruptly switches directions to balance extra Lorentz forces from 3D circulations of electric current. These circulations appear near sudden expansions including the large expansion at $x/b = 1$ and the channel exits at $x/b = 4$. By contrast, 3D MHD effects at a sudden contraction like the entrance to the multiple channels at $x/b = 2$ cause a peak in the pressure distribution. The peaks are caused by 3D electric currents which circulate in the opposite direction as near sudden expansions. 3D MHD effects at expansions and contractions produce an extra pressure loss called the 3D MHD pressure drop as discussed in Sec. III B. This loss is expected to be small when r_{exp} (or $n \times s_c$) is close to 1. Here, $n \times s_c$ is 0.9 so the 3D MHD pressure drops from the channel ends are small and the differences in the pressure drop between cases with and without channels are less than 10%. When $r_{\text{exp}} \sim 10$ as in DCLL manifolds, the 3D MHD pressure drops account for nearly half the pressure drop across the entire liquid metal loop (Sec. III E). Having demonstrated that the influences of the multiple channels are small provided that $n \times s_c \sim 1$, ducts featuring a sudden expansion without multiple channels were simulated for a range of r_{exp} , Ha , and N in order to study the 3D MHD pressure drop. These simulations' results are discussed below.

Electrically non-conducting ducts featuring a sudden expansion were simulated for a range of $r_{\text{exp}} = [4, 6, 8, 10, 12]$, $1000 \leq Ha \leq 6570$, $1918.44 \leq N \leq 863298$, and $50 \leq Re \leq 2500$. The 3D MHD pressure

drop was determined for the 96 simulations by subtracting the effective 2D pressure drops (calculated using Shercliff's pressure formula) from the pressure drop of each simulation. These data were then sorted into groups with equal r_{exp} , then curve fitted to linear functions of either $NHa^{-1/2}$ or $N^{2/3}$. The slopes, k_{ve} , k_{ie} , and offsets, d_{ve} , d_{ie} , of these linear functions were then curve fitted as functions of expansion ratio. The resulting formulas can be used to predict the 3D MHD pressure drop for a wide range of parameters and are shown as follows:

$$\Delta P_{3D} = \frac{\rho U^2}{2} (k_{ve} NHa^{-1/2} + d_{ve}) \text{ for } Ha^{3/2}/N < 3, ($$

$$\Delta P_{3D} = \frac{\rho U^2}{2} (k_{ie} N^{2/3} + d_{ie}) \text{ for } Ha^{3/2}/N > 3. (8)$$

Here, k_{ve} , d_{ve} , k_{ie} , and d_{ie} are functions of the expansion ratio, r_{exp} ,

$$k_{ve} = 0.31r_{\text{exp}} + 3.08, (9)$$

$$d_{ve} = 342.92r_{\text{exp}} - 1563.85, (10)$$

$$k_{ie} = 0.33r_{\text{exp}} + 1.19, (11)$$

$$d_{ie} = -11.55r_{\text{exp}}^2 + 85.43r_{\text{exp}} - 264.39. (12)$$

Equations (7)–(12) describe the 3D pressure drop in both the viscous-electromagnetic and inertial-electromagnetic regimes. Figure 13 shows the pressure model plotted against the computed results that were used in its making. The RMSD [root-mean-square deviation (not normalized)] and R^2 (coefficient of determination) were also calculated, demonstrating good agreement of the proposed pressure model with the computed pressure drops.

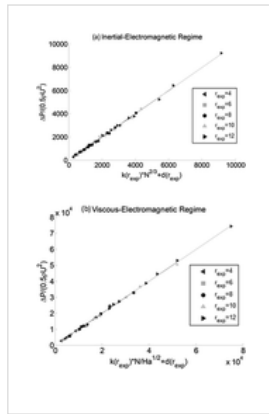


FIG. 13.

Proposed pressure model for MHD flows in a non-conducting manifold. (a)

For the IE regime ($Ha^{3/2}/N > 3$), the RMSD and R2 is 76.08 and 0.9980, respectively. (b) For the VE

regime ($Ha^{3/2}/N < 3$), the RMSD and R2 for the fit is 540.9 and 0.9989, respectively.

[↓ PPT](#) | [High-resolution](#)

D. Flow distribution analysis

For the purpose of characterizing the flow distribution among the parallel channels, it is useful to consider two parameters: one is the length of the expansion region and the second is the length of the parallel channels themselves. Here, we investigate the effect of the length of the expansion region on the flow distribution for the case of short, non-conducting channels for various flow parameters ($Ha \sim 10^3$ and $Re \sim 10^1-10^3$) and expansion ratios ($r_{exp} = 4-12$). According to our observations, if the parallel channels begin before the reattachment length introduced in Sec. III B, the flow distribution will be significantly biased toward the center channels. More flow enters central channels because the stagnation pressure at the channel walls interrupts the redistribution of flow which occurs near the side walls before the reattachment length. Alternatively, if the expansion length is greater than the reattachment length, the flow distribution will be well balanced. This phenomenon is illustrated in Fig. 14.

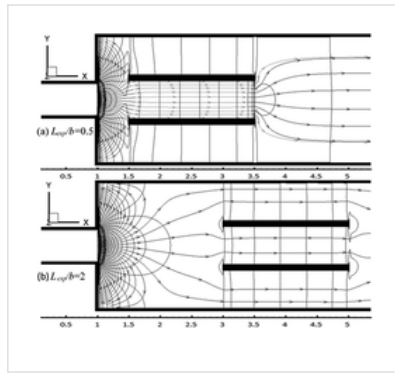


FIG. 14.
Velocity streamlines are plotted with pressure contour lines on the sidewall ($z/a = 0.98$) for two

manifold geometries. $Ha = 1465$, $Re = 50$, $r_{exp} = 4$, $L_{chan}/b = 2$, $s_c = 0.3$, and $L_{exp}/b = 0.5$ or 2 for (a) and (b), respectively.

[↓ PPT | High-resolution](#)

Here, the percentage of the flow through the center channel is 41.0% and 33.3% for $L_{exp}/b = 0.5$ and 2 , respectively, and the reattachment length, non-dimensionalized by b , is approximately 0.8 . Note that for three channels, 33.3% is perfectly balanced. The relationship between L_{exp}/b and flow distribution will be quantified later in this section after discussing the relative importance of flow parameters.

Electrically non-conducting manifolds featuring a sudden expansion were simulated to study how the flow distribution produced by a manifold changes with flow parameters and geometry. Once the simulations converged, the axial velocity component was integrated over each channel's cross section using Simpson's method. We divided the result by the total flow rate to determine the percentage of the flow through each channel. For the first batch of simulations, manifolds with $r_{exp} = 4$, $L_{chan}/b = 2$, and $n = 3$ channels were considered (as depicted in Fig. 1). These simulations included a range of $L_{exp}/b = [0.5, 1, 2, 3]$ and $Ha \sim [1000, 1500, 2000]$. Additionally, for each combination of L_{exp} and Ha , between 3 and 5 choices of Re were included

over a range of $50 \leq Re \leq 3750$. The difference in the percentage of the flow through each side channel was calculated to be at most on the order $10^{-3}\%$, thus confirming the symmetry of the flow for our parameter space. Figure 15 shows the percentage of the flow through the center channel for each set of parameters.

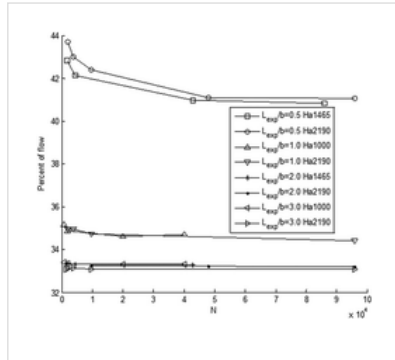


FIG. 15. Percentage of flow through the center channel of manifolds with three channels is plotted for various Ha , N , and

L_{exp} . For these simulations, $r_{\text{exp}} = 4$ and $L_{\text{chan}}/b = 2$.

[↓ PPT | High-resolution](#)

For the chosen parameter space, the variable to have the biggest impact on flow distribution is L_{exp} . On the other hand, halving Ha or increasing Re by a factor of 50 produced $O(1\%)$ or smaller differences in flow distribution. As explained in Sec. III B, a 3D flow structure attached to the side walls is the primary mechanism for flow redistribution and it penetrates into the expansion region a distance that scales with $N^{-1/3}$ ¹² in the IE regime and possibly $Ha^{-1/2}$ in the VE regime based on the arguments in Ref. 7. Thus for large N and Ha , this distance becomes increasingly insensitive to N and Ha .

One of our hypotheses is that the channels influence flow distribution in part by interrupting the redistribution of flow occurring in the expansion region near the side walls. In the present study, the channels are short enough such that the

length of the channels almost does not affect the flow balancing and the overall MHD pressure drop. This is done to mostly observe the effects of the flow physics inside the expansion region on the flow balance of the manifold without being masked by the channel length effect. We tested this hypothesis by simulating a manifold without multiple channels and measuring the percentage of flow in the center third of the duct at 4 distances L downstream of the sudden expansion equal to $L/b = [0.5, 1, 2, 3]$ for $Ha = 2190$, $Re = 500$, and $r_{exp} = 4$. We then compared these values with the percentage of flow through the center channel in manifolds with three channels that begin a distance downstream of the sudden expansion equal to $L_{exp}/b = [0.5, 1, 2, 3]$ for the same Ha , Re , and r_{exp} . The results of this comparison are shown in Fig. 16. Note that while calculating the integrals of axial velocity, some values were linearly interpolated because dividing the duct into even thirds split cells for the manifolds without channels.

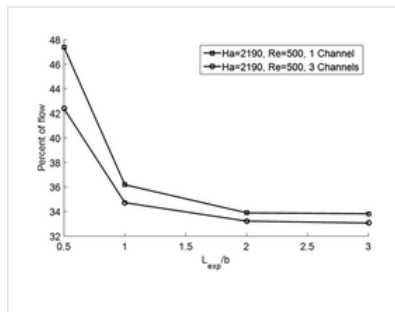


FIG. 16. Percentage of flow through the center channel of manifolds with three channels

and manifolds without multiple channels is plotted for various $L_{exp} = L$. For these simulations, $r_{exp} = 4$ and, for simulations with channels, $L_{chan}/b = 2$.

[↓ PPT](#) | [High-resolution](#)

The differences in the percentage of the flow for the two cases are within 5% with the manifold having three channels being slightly more balanced.

This is the expected result because the channels induce a small balancing effect via 2D MHD pressure drops within the channels that are dependent on the local average velocity. The results shown in Fig. 16 justify using a single simulation of a manifold without channels to predict the flow distributions of manifolds with $n > 2$ short channels which begin after any desired length in the expansion region, L_{exp} . This method makes comparison of multiple manifold designs much less expensive. Electrically non-conducting ducts featuring a sudden expansion without multiple channels were simulated for a range of r_{exp} , Ha , and Re in order to study the flow distribution in manifolds with multiple channels. These simulations' results are discussed.

Manifold flows with $Re = 1000$ and $r_{\text{exp}} = 8$ were simulated for four choices of $Ha = [2000, 3000, 3400, 4380]$ to study how the flow distribution at various locations downstream of the expansion changes with Ha . The results are plotted in Fig. 17 as the percentage of flow through the center third of the duct versus L/b where L is the axial distance downstream of the sudden expansion where the flow distribution is calculated.

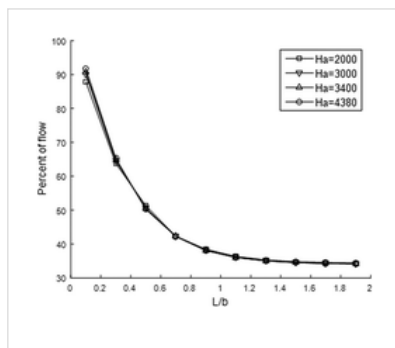


FIG. 17. Percentage of flow through the center virtual channel of manifolds with three virtual

channels is plotted for various distances L/b into the expansion region for four choices of Ha . Here, $r_{\text{exp}} = 8$ and $Re = 1000$.

[↓ PPT](#) | [High-resolution](#)

In this parameter space, the flow distribution is weakly dependent on Ha . As before, the distance downstream is the most important factor for determining the flow distribution for this parameter space and now an exponential decay of flow unbalance is apparent along the axial direction.

Manifold flows with $Ha = 5475$ and $r_{\text{exp}} = 10$ were simulated for six choices of $Re = [50, 100, 500, 1000, 1500, 2000]$ to study how the flow distribution at various locations downstream of the expansion changes with Re . The results are plotted in Fig. 18 as the percentage of the flow through the center third of the duct versus L/b .

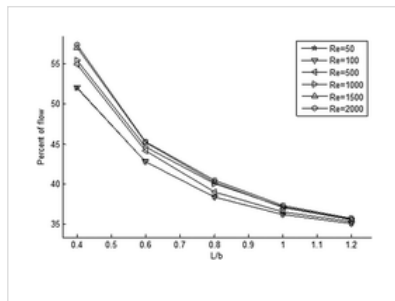


FIG. 18. Percentage of flow through the center virtual channel of manifolds with

three virtual channels is plotted for various distances L/b into the expansion region and at multiple Re . Here, $r_{\text{exp}} = 10$ and $Ha = 5475$.

[↓ PPT](#) | [High-resolution](#)

The flow becomes less balanced and more flow is in the center third of the duct as Re increases. This behavior is also in agreement with the cases with multiple channels shown in Fig. 15.

Electrically non-conducting manifolds were simulated with $Re = 2000$, $Ha = 547.5r_{\text{exp}}$, and 4 choices of $r_{\text{exp}} = [6, 8, 10, 12]$ in order to determine the effect of expansion ratio on flow distribution. As with all the simulations in the present work, d is

fixed so the value b changes linearly with r_{exp} . Ha also varies with r_{exp} because each simulation in this batch has the same magnetic field and fluid electrical conductivity. For each simulation, the flow distribution was calculated at 8 locations evenly spaced in the axial direction from $L = 0.025$ m to 0.2 m for 3, 10, and 12 virtual channels. Then we curve fitted the percentage of flow through the center virtual channels to an exponential function of L as shown in the following equation:

$$\text{Percentage of flow in center} = Ae^{BL} + C, \quad (13)$$

where A , B , and C are dependent on r_{exp} and n only. We found that the RMSDs for the exponential curve fits were smaller than those for power law fits ($\% = DL^E + F$ where D , E , and F are dependent on r_{exp} and n only) of the same data and that the RMSD was $O(0.1\%)$ indicating a good fit. The resulting values for A , B , and C were thus determined for each expansion ratio as shown in Fig. 19.

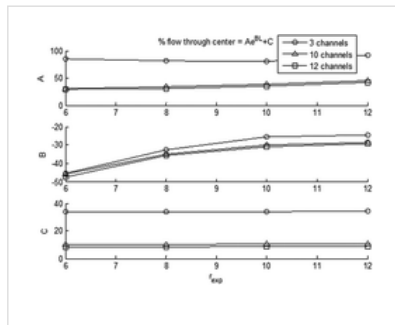


FIG. 19. The parameters A , B , and C plotted versus r_{exp} for the exponential functions

describing the percentage of the flow through the center virtual channel versus L for manifolds with 3, 10, and 12 virtual channels. $Ha = 547.5r_{\text{exp}}$ and $Re = 2000$.

[↓ PPT | High-resolution](#)

The offset C showed no dependence on r_{exp} which makes sense because as L increases, the flow distribution approaches a balanced state. Here, $C \sim$

34%, 10.3%, and 8.6% for 3, 10, and 12 channels, respectively. For a perfectly balanced flow, the percentage of the flow in each channel would be 33.33%, 10%, and 8.33%, respectively. Using the exponential functions determined above, we estimated the balancing length L^*/b which we define as the non-dimensionalized axial distance downstream of the sudden expansion where the percentage of flow through the center virtual channel equals $C + 0.1C$. The estimations for balancing lengths for $Re = 2000$, $Ha = 547.5r_{\text{exp}}$, and $r_{\text{exp}} = [6, 8, 10, 12]$ are plotted in Fig. 20.

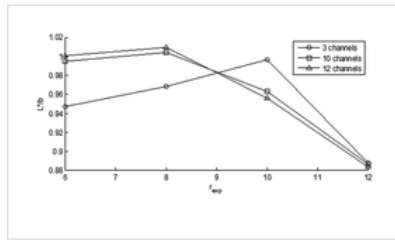


FIG. 20. The balancing length is plotted versus r_{exp} for manifolds with 3,

10, and 12 virtual channels. $Ha = 547.5r_{\text{exp}}$ and $Re = 2000$.

[PPT](#) | [High-resolution](#)

For $r_{\text{exp}} = 12$, the manifold flow is estimated to be balanced within $L/b = 0.9$ for any number of channels. For all the cases evaluated above, the conclusion $L^*/b \leq 1$ can be drawn.

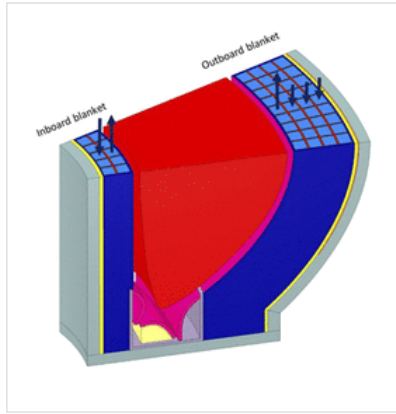
E. Example of application of the derived pressure model to a fusion blanket

Here, the obtained formulas for the 3D MHD pressure drop in a manifold, Eqs. (7)–(12), are applied to a DCLL blanket design. In the recent FNSF (Fusion Nuclear Science Facility) study in the US,³¹ a DCLL blanket was designed for both inboard (IB) and outboard (OB) regions (Fig. 21). The entire

machine is subdivided into 16 toroidal sectors, such that there are 16 inboard (IB) and 16 outboard (OB) blankets. Each sector with the blankets can be removed via an individual port using a horizontal maintenance scheme. In the IB blanket, the eutectic PbLi alloy flows upwards in the five front ducts facing the plasma, makes a U-turn at the top of the blanket, and then flows downwards in the five rear ducts. The flows occur in the presence of a strong plasma-confining magnetic field resulting in a high MHD pressure drop in the flowing liquid breeder. There are two manifolds at the bottom of the blanket to feed the poloidal ducts and to collect the hot PbLi at the exit of the blanket. The OB blanket has a similar structure but the number of the ducts and blanket dimensions are different to fit into a larger space at the OB. The entire blanket, including the manifolds, has electrically insulating flow channel inserts made of silicon carbide ceramics³² to reduce the MHD pressure drop, such that the present model that assumes electrically insulating walls is applicable. In this particular example, we limit our considerations of the MHD pressure drop to that in the inlet manifold of the IB blanket. More results for manifold flows are presented in Ref. 33. For the reference blanket,³³ the magnetic field is 10 T, the poloidal length is 7 m, and the toroidal width is 1.69 m. The PbLi velocity in the expansion section of the manifold is 0.076 m/s and the flow absorbs 0.78 MW/m² of heat generated by neutrons. The dimensionless flow parameters and the computed MHD pressure drop are summarized in Table II.

FIG. 21.

Cross-cut of one of the 16 toroidal sectors in the FNSF with the IB and OB blankets. The arrows show the PbLi flow path in the poloidal ducts.



↓ PPT | High-resolution



TABLE II. The dimensionless blanket parameters and the computed 3D MHD pressure drop in the manifold.

As discussed in Sec. III C, the 3D MHD pressure drop (in the MHD scale) was found to scale as $Ha^{-1/2}$ in the VE regime and $N^{-1/3}$ in the IE regime for electrically non-conducting manifolds with sudden expansions. Here, it was found that $Ha^{3/2}/N > 3$. This suggests that the flow in the manifold is in the inertial-electromagnetic regime. The computed MHD pressure drop of 0.196 MPa in the inlet manifold flow is about 20% of the overall PbLi pressure drop in the blanket. Taking into account that the blanket has two manifolds, the associated pressure drop due to 3D effects in the manifold flows approaches nearly half of the blanket pressure drop. This fact really justifies the importance of the obtained pressure drop correlations.

IV. CONCLUDING REMARKS

As seen from the analyses above, the flow physics in a manifold are dominated by 3D effects. Formation of internal shear layers at the locations where the flow experiences expansions or contractions in the plane parallel to the applied magnetic field is the

most important manifestation of the 3D effects as it affects the flow and pressure field and eventually becomes responsible for a high 3D MHD pressure drop. As suggested in this study, an effective way of identifying such internal layers, which is a place of many interesting effects, is to plot the magnitude of the curl of the induced Lorentz force. It also helps to distinguish between the internal shear layers and inviscid, irrotational core flows, where the electromagnetic force is fully balanced by the pressure gradients and the curl of the Lorentz force is correspondingly small. Applying this technique to the flow in the manifold suggests that the internal shear layers are formed at the sudden expansion and also at the entry to and exit from the parallel channels. Of them, the internal shear layer at the sudden expansion is the main source of 3D MHD effects.

In designing manifolds for fusion applications, the 3D MHD effects which influence the pressure and the flow distribution cannot be ignored. These effects are caused by 3D electric currents which form near expansions and contractions parallel to the applied magnetic field. The Lorentz force field is rotational at these locations and since pressure gradients are not rotational, hydrodynamic forces must develop to balance the electromagnetic force. Ultimately, 3D flow structures form and this results in extra pressure losses.

A 3D MHD pressure drop resulting from 3D MHD effects is inserted into the pressure distribution which accounts for a significant portion of the pressure drop across the liquid metal loop. In Sec. [III C](#), pressure correlations informed by scaling analysis were introduced and it was shown that the 3D MHD pressure drop scales linearly with r_{exp} and, depending on the size of N relative to $Ha^{3/2}$, either $\rho U^2 N^{2/3}$ in the IE regime or $\rho U^2 N Ha^{-1/2}$ in the VE

regime. A similar pressure drop is expected for an outlet manifold featuring a sudden contraction. While this claim is likely to be true for the VE regime, the pressure drop may change significantly for the IE regime because while Lorentz and viscous forces are reversible, inertial forces are not. Future studies are therefore necessary as fusion blankets will operate firmly inside the IE regime.

3D MHD effects at sudden expansions are also responsible for the occurrence of a complex flow structure which quickly redistributes the flow along the transverse direction downstream of the sudden expansion. In Sec. III D, it was discussed that the flow distribution among short parallel channels is mostly controlled by the length of the expansion region for Ha and $N \gg 1$, particularly when the expansion region ends before the flow becomes fully developed. Results for $r_{\text{exp}} = 12$, $Ha = 6570$, and $N = 21\,582$ indicate that MHD manifold flows at even higher Ha and N will feature a balanced flow distribution so long as the channels begin after a length $L_{\text{exp}}/b = 1$ downstream of the expansion. However, if the walls are electrically conducting, multi-channel effects such as the Madarame effect and electromagnetic coupling can impact the flow distribution and the MHD pressure drop.^{2,29,30} These effects account for phenomena associated with electric currents that connect through two or more parallel channels when the channels are stacked perpendicular or parallel to the magnetic field, respectively. When the walls are non-conducting, as in the present work, multi-channel effects can obviously be neglected.

It should be mentioned that the proposed manifold model has a simpler geometry compared to the “real” blanket manifold where the flow turns from the radial to the poloidal direction right after the expansion region. This feature is not included here

as the change in the flow direction from radial to poloidal in the real blanket occurs in the plane perpendicular to the applied magnetic field such that associated changes in the MHD pressure drop are known to be small.⁹ The outlet region at the exit of the manifold is another special feature of the proposed model. It was added to the model mostly because of the computational reasons to minimize the downstream effect of the outlet boundary condition on the flow inside the manifold. Also, in a real manifold design, the height of the expansion region can be different from the size of the feeding duct. The real manifold may also need rounded corners in the expansion region to provide a smooth transition from the flow in the inlet pipe to that in the expansion region. This will result in a lower MHD pressure drop in the manifold by reducing 3D effects.³⁴ In spite of these simplifications, the proposed model preserves the most important features of the real manifold flow. Future studies might be needed to include such details in the computational model in a design phase, but this will hardly change the main conclusions of the present study about the fundamental flow physics associated with the 3D MHD effects as described in this research.

The analysis done in this study covers a range of flow parameters significantly lower compared to those of real blanket flows. In this range, the flow was found to be laminar while the blanket flows are expected to demonstrate quasi-2D (Q2D) turbulence.³⁵ In Q2D turbulent flows, turbulent vortices are big (comparable in size with the duct dimension) coherent structures stretched along magnetic field lines between the two Hartmann layers at the flow confining walls. Such vortices are known to have low Joule and negligible viscous dissipation due to their orientation with respect to

the magnetic field.³⁶ Therefore, the contribution of the Q2D vortices in the MHD pressure drop seems to be much smaller compared to other pressure-affecting factors, first of all the internal shear layer at the expansion as studied here. Though Eqs. (7)–(12) were determined for steady laminar MHD flows, these formulas will likely need only small corrections to account for turbulence effects.

ACKNOWLEDGMENTS

This work was performed with support from the US Department of Energy, Office of Fusion Energy Sciences, under Grant No. DE-FG02-86ER52123.

This work used computational and storage services associated with the Hoffman2 Shared Cluster provided by the UCLA Institute for Digital Research and Education's Research Technology Group.

REFERENCES

1.
S. Smolentsev, N. Morley, M. Abdou, and S. Malang, "Dual-coolant lead-lithium (DCLL) blanket status and R&D needs," *Fusion Eng. Des.* **100**, 44–54 (2015).
<https://doi.org/10.1016/j.fusengdes.2014.12.031>,
[Google Scholar](#), [Crossref](#), [CAS](#)

2.
S. Smolentsev, R. Moreau, L. Buhler, and C. Mistrangelo, "MHD thermofluid issues of liquid-metal blankets: Phenomena and advances," *Fusion Eng. Des.* **85**(7-9), 1196–1205 (2010).
<https://doi.org/10.1016/j.fusengdes.2010.02.038>,
[Google Scholar](#), [Crossref](#), [CAS](#)

3.

J. Shercliff, "Steady motion of conducting fluids in pipes under transverse magnetic fields," *Math. Proc. Cambridge Philos. Soc.* **49**, 136–144 (1953).

<https://doi.org/10.1017/s0305004100028139>,

[Google Scholar](#), [Crossref](#)

4.

J. Hunt, "Magnetohydrodynamic flow in rectangular ducts," *J. Fluid Mech.* **21**(04), 577–590 (1965).

<https://doi.org/10.1017/s0022112065000344>,

[Google Scholar](#), [Crossref](#)

5.

S. Smolentsev, C. Wong, S. Malang, M. Dagher, and M. Abdou, "MHD considerations for the DCLL inboard blanket and access ducts," *Fusion Eng. Des.* **85**(7-9), 1007–1011 (2009).

<https://doi.org/10.1016/j.fusengdes.2009.12.005>,

[Google Scholar](#), [Crossref](#)

6.

G. Branover, A. Vasil'ev, and Y. Gel'fgat, "Effect of a transverse magnetic field on the flow in a duct at a sudden cross section enlargement," *Magn. Gidrodin.* **3**(3), 61–65 (1967). [Google Scholar](#)

7.

J. Hunt and S. Leibovich, "Magnetohydrodynamic flow in channels of variable cross-section with strong transverse magnetic fields," *J. Fluid Mech.* **28**(2), 241–260 (1967).

<https://doi.org/10.1017/s0022112067002046>,

[Google Scholar](#), [Crossref](#)

8.

U. Müller and L. Büller, *Magnetohydrodynamics in Channels and Containers* (Springer Science & Business Media, 2001), pp. 83–97. [Google Scholar](#), [Crossref](#)

9.

S. Molokov, “Liquid metal flows in manifolds and expansions of insulating rectangular ducts in the plane perpendicular to a strong magnetic field,” KfK-5272, Kernforschungszentrum Karlsruhe, 1994.

[Google Scholar](#)

10.

R. Stieglitz, L. Barleon, L. Bühler, and S. Molokov, “Magnetohydrodynamic flow in a right-angle bend in a strong magnetic field,” *J. Fluid Mech.* **326**, 91–123 (1996). <https://doi.org/10.1017/s0022112096008257>,

[Google Scholar](#), [Crossref](#)

11.

L. Bühler and S. Horanyi, “Experimental investigations of MHD flows in a sudden expansion,” WIS B, FKA, 7245, 2006, pp. 1–65. [Google Scholar](#)

12.

C. Mistrangelo, “Three-dimensional MHD flow in sudden expansions,” Ph.D. dissertation, No. FZKA (Forschungszentrum Karlsruhe GmbH, 2006).

[Google Scholar](#)

13.

T. Rhodes, S. Smolentsev, and M. Abdou, “Effect of the length of the poloidal ducts on flow balancing in a liquid metal blanket,” *Fusion Eng. Des.* (published online).

<https://doi.org/10.1016/j.fusengdes.2018.04.019>,

[Google Scholar](#)

14.

S. Smolentsev, N. Morley, M. Abdou, R. Munipalli, and R. Moreau, "Current approaches to modeling MHD flows in the dual coolant lead lithium blanket," *Magnetohydrodynamics* **42**(2-3), 225–236 (2006).

[Google Scholar](#)

15.

M. Ni, R. Munipalli, N. Morley, P. Huang, and M. Abdou, "A current density conservative scheme for incompressible MHD flows at a low magnetic Reynolds number. Part I: On a rectangular collocated grid system," *J. Comput. Phys.* **227**, 174–204 (2007).

<https://doi.org/10.1016/j.jcp.2007.07.025>,

[Google Scholar](#), [Crossref](#)

16.

M. Ni, R. Munipalli, P. Huang, N. Morley, and M. Abdou, "A current density conservative scheme for incompressible MHD flows at a low magnetic Reynolds number. Part II: On an arbitrary collocated mesh," *J. Comput. Phys.* **227**, 205–228 (2007).

<https://doi.org/10.1016/j.jcp.2007.07.023>,

[Google Scholar](#), [Crossref](#)

17.

R. Munipalli, S. Shankar, M. Ni, and N. Morley, "Development of a 3-D incompressible free surface MHD computational environment for arbitrary geometries: HIMAG," DOE SBIR Phase-II Final Report, 2003. [Google Scholar](#)

18.

K. Messadek and M. Abdou, "Experimental study of MHD flows in a prototypic inlet manifold section of the DCLL test blanket module,"

Magnetohydrodynamics **45**(2), 233–238 (2009).

[Google Scholar](#)

19.

N. Morley, R. Munipalli, P. Huang, and M. Abdou, "MHD simulations of liquid metal flow through a toroidally oriented manifold," *Fusion Eng. Des.* **83**(7–9), 1335–1339 (2008).

<https://doi.org/10.1016/j.fusengdes.2008.04.010>,

[Google Scholar](#), [Crossref](#), [CAS](#)

20.

L. Bühler, "Inertialess magnetohydrodynamic flow in expansions and contractions," FZKA, FZKA 6904, 2003. [Google Scholar](#)

21.

J. Hunt and R. Holroyd, *Applications of Laboratory and Theoretical MHD Duct Flow Studies in Fusion Reactor Technology* (HM Stationery Office, 1977).

[Google Scholar](#)

22.

A. Kulikovskii, "Slow steady flows of a conducting fluid at large Hartmann numbers," *Fluid Dyn.* **3**(2), 1–5 (1971). <https://doi.org/10.1007/bf01013541>,

[Google Scholar](#), [Crossref](#)

23.

Y. Gelfgat and L. Kit, "Investigation of the conditions of occurrence of M-shaped velocity profiles at sudden expansion or contraction of a magnetohydrodynamic flow,"

Magnetohydrodynamics **7**(1), 21–25 (1971).

[Google Scholar](#)

24.

G. Branover and E. Shcherbinin,
“Magnetohydrodynamic jet flow in a bounded
space,” *Magn. Gidrodin.* **2**, 55–63 (1966).

[Google Scholar](#)

25.

J. Walker, G. Ludford, and J. Hunt, “Three-
dimensional MHD duct flows with strong
transverse magnetic fields. Part 3. Variable-area
rectangular ducts with insulating walls,” *J. Fluid
Mech.* **56**(01), 121–141 (1972).

<https://doi.org/10.1017/s0022112072002228>,

[Google Scholar](#), [Crossref](#)

26.

T. Aitov, A. Kalyutik, and A. Tananaev, “Numerical
analysis of three dimensional MHD flow in channel
with abrupt change of cross section,”
Magnetohydrodynamics **19**(2), 223–229 (1983).

[Google Scholar](#)

27.

B. Picologlou, C. Reed, T. Hua, L. Barleon, H.
Kreuzinger, and J. Walker, “MHD flow tailoring in
first wall coolant channels of self-cooled blankets,”
Fusion Eng. Des. **8**, 297–303 (1989).

[https://doi.org/10.1016/s0920-3796\(89\)80121-8](https://doi.org/10.1016/s0920-3796(89)80121-8),

[Google Scholar](#), [Crossref](#), [CAS](#)

28.

M. Myasnikov and A. Kalyutik, “Numerical
simulation of incompressible MHD flows in
channels with a sudden expansion,”
Magnetohydrodynamics **33**(4), 342–349 (1997).

[Google Scholar](#), [CAS](#)

29.

Q. Hua and B. Picologlou, "Magnetohydrodynamic flow in a manifold and multiple rectangular coolant ducts of self-cooled blankets," *Fusion Sci. Technol.* **19**(1), 102–112 (1991).

<https://doi.org/10.13182/fst91-a29320>,

[Google Scholar](#), [Crossref](#), [CAS](#)

30.

H. Chen, Z. Meng, J. Feng, and Q. He, "Effect of electromagnetic coupling on MHD flow in the manifold of fusion liquid metal blanket," *Fusion Eng. Des.* **89**(7-8), 1406–1410 (2014).

<https://doi.org/10.1016/j.fusengdes.2014.01.023>,

[Google Scholar](#), [Crossref](#), [CAS](#)

31.

C. Kessel, J. Blanchard, A. Davis, L. El-Guebaly, N. Ghoniem, P. Humrickhouse *et al.*, "The fusion nuclear science facility, the critical step in the pathway to fusion energy," *Fusion Sci. Technol.* **68**, 225–236 (2015). <https://doi.org/10.13182/fst14-953>,

[Google Scholar](#), [Crossref](#)

32.

S. Smolentsev, M. Abdou, N. B. Morley, S. Malang, and C. Kessel, "R&D needs and approach to measure progress for liquid metal blankets and systems on the pathway from present experimental facilities to FNSF," *Fusion Sci. Technol.* **68**, 245–250 (2015).

<https://doi.org/10.13182/fst14-919>, [Google Scholar](#),

[Crossref](#)

33.

S. Smolentsev, T. Rhodes, G. Pulugundla, C. Courtessole, M. Abdou, S. Malang, M. Tillack, and C. Kessel, “MHD thermohydraulics analysis and supporting R&D for DCLL blanket in the FNSF,” *Fusion Eng. Des.* (published online).

<https://doi.org/10.1016/j.fusengdes.2017.06.017>,

[Google Scholar](#)

34.

C. Mistrangelo and L. Bühler, *MHD Flow in a Prototypical Manifold of DCLL Blankets* (KIT Scientific Publishing, 2014), p. 7673. [Google Scholar](#)

35.

S. Smolentsev, N. Vetcha, and M. Abdou, “Effect of a magnetic field on stability and transitions in liquid breeder flows in a blanket,” *Fusion Eng. Des.* **88**, 607–610 (2013).

<https://doi.org/10.1016/j.fusengdes.2013.04.001>,

[Google Scholar](#), [Crossref](#), [CAS](#)

36.

U. Burr, L. Barleon, U. Muller, and A. Tsinober, “Turbulent transport of momentum and heat in magnetohydrodynamic rectangular duct flow with strong sidewall jets,” *J. Fluid Mech.* **406**, 247–279 (2000). <https://doi.org/10.1017/s0022112099007405>

, [Google Scholar](#), [Crossref](#), [CAS](#)

Published by AIP Publishing.



Resources

[AUTHOR](#)

[LIBRARIAN](#)

[ADVERTISER](#)

General Information

[ABOUT](#)

[CONTACT](#)

[HELP](#)

[PRIVACY POLICY](#)

[TERMS OF USE](#)

FOLLOW AIP PUBLISHING:



Website © 2019 AIP Publishing LLC. Article copyright remains as specified within the article.

Scitation